ANTIMICROBIALS

Antibacterial activity of nonantibiotics is orthogonal to standard antibiotics

Mariana Noto Guillen, Carmen Li, Brittany Rosener, Amir Mitchell*

Numerous nonantibiotic drugs have potent antibacterial activity and can adversely affect the human microbiome. The mechanistic underpinning of this toxicity remains largely unknown. We investigated the antibacterial activity of 200 drugs using genetic screens with thousands of barcoded *Escherichia coli* knockouts. We analyzed 2 million gene-drug interactions underlying drug-specific toxicity. Network-based analysis of drug-drug similarities revealed that antibiotics clustered into modules that are consistent with the mode of action of their established classes, whereas nonantibiotics remained unconnected. Half of the nonantibiotics clustered into separate modules, potentially revealing shared and unexploited targets for new antimicrobials. Analysis of efflux systems revealed that they widely affect antibiotics and nonantibiotics alike, suggesting that the impact of nonantibiotics on antibiotic cross-resistance should be investigated closely in vivo.

Our microbiomes play a critical role in maintaining our health and can affect the efficacy of various therapeutics. Studies have revealed that the effectiveness of many drugs not traditionally prescribed for treating bacterial infections, called nonantibiotics hereafter, can be affected by drug-microbiome interactions, including bacterial-driven drug metabolism (*1*–*3*) and bioaccumulation (*4*). Complementary studies of nonantibiotics have also investigated the reciprocal effect: how nonantibiotic drugs might disrupt the microbiome and potentially culminate in dysbiosis, a detrimental disruption of the host's microbiome. Recent works revealed that multiple nonantibiotics are associated with shifts in microbiome species composition (*5*, *6*). Examples include antidiabetics (*7*), proton-pump inhibitors (*8*, *9*), antipsychotics (*10*), and nonsteroidal anti-inflammatory drugs (*11*). Although the mechanisms underlying these associations are complex, direct drug-bacterial interactions are thought to be one key force mediating these shifts (*2*). A recent in vitro screen revealed that roughly a quarter of nonantibiotics are potent antibacterials at physiologically relevant concentrations (*12*).

A key question that arises from the observation of widespread antibacterial activity of nonantibiotics is the underlying mode of action in bacteria. Work on even very well-characterized drugs, such as the chemotherapy agent fluorouracil (*13*–*16*), demonstrated that they can have both shared and distinctive toxicity mechanisms across phylogenetic kingdoms. Uncovering the mode of action across a wide panel of nonantibiotic drugs has the potential to identify both common and distinct toxicity mechanisms with standard antibiotic drug classes, both of which have important biomedical implications. Previously unrecognized toxicity mechanisms may identify unexploited targets for future antibiotic development, and shared toxicity mechanisms can identify drugs that could inadvertently select for multidrug resistance under chronic administration and may undermine the efficacy of antibiotics.

Motivated by reports of nonantibiotics' widespread antibacterial activity, we used an *Escherichia coli* lab strain as a platform to uncover the pathways underlying bacterial growth inhibition. We used a pooled genetic screening approach to investigate a panel of almost 200 drugs. Our screens yielded more than 2 million bacterial fitness measurements and permitted analysis that extended beyond individual drug-gene interactions. We discovered that nonantibiotics operate through toxicity mechanisms that are orthogonal to standard antibiotics. Conversely, we found that knockout of efflux systems increased sensitivity against most antibiotics and nonantibiotics. Follow-up lab evolution experiments with three nonantibiotics supported the main conclusions of our analysis by demonstrating that evolved resistance can culminate in broad antibiotic cross-resistance and by uncovering a bacterial-translation initiation factor, initiation factor 2 (IF2), as a previously unknown cellular target that is not currently exploited by standard antibiotics.

Results

Drug screen reveals nonantibiotics with antibacterial activity

To identify drugs with antibacterial activity, we tested the effects of 1280 drugs (226 antibiotics and 1054 nonantibiotics) on *E. coli* growth in defined media (Fig. 1A). This panel includes approved and investigational drugs, as well as 26 nutraceutical compounds (table S1A). We monitored culture density over multiple hours and used a permissive cutoff for identifying growth inhibition—1 SD below the median optical density of control cultures. We identified 176 nonantibiotics and 142 antibiotics that were inhibitory at a 10-μM drug concentration. Absence of antibacterial activity of some antibiotics may arise from their restricted phylogenetic spectrum as reflected by the annotated affected organism (table S1A). We validated the antibacterial activity of the selected drugs in a similar follow-up screen with four replicates and a strict statistical cutoff. We validated that 104 nonantibiotics significantly inhibited growth [one-tailed t test, false discovery rate (FDR)–adjusted P value of 0.25]. Figure 1B and tables S1, B to D, show a summary of the number of hits identified in the screens. We focused on the 103 most toxic antibiotics and the 83 most toxic nonantibiotics for further analysis (supplementary materials, materials and methods).

We next tested if the antibacterial activity of nonantibiotics can be attributed to chemical similarity to standard antibiotics. We measured the chemical similarity of each drug pair by calculating the Tanimoto coefficient with Morgan2 fingerprints (*17*, *18*). This measurement denotes the proportion of shared chemical features between two molecules (values >0.8 are typically considered highly similar). Figure 1D and table S2 show the coefficients of the top 186 most toxic drugs ordered by their classes. Overall, we observed high chemical similarity between antibiotics that target the same cellular process (Fig. 1D, dark triangles). We observed low chemical similarity for drug pairs belonging to different antibiotic classes or pairs with at least one nonantibiotic (Fig. 1D, light colors). The histograms of chemical similarity coefficients across different groups revealed highly dissimilar distributions (Fig. 1E). We used these distributions to define a lower (permissive) cutoff for chemical similarity. Hence, antibacterial activity of nonantibiotics is not necessarily a result of chemical similarity to standard antibiotics.

Pooled genetic screen for identifying modulators of toxicity

We next employed a pooled genetic screening method that we previously developed (*15*, *19*, *20*) to identify the cellular pathways modulating the antibacterial activity of 186 drugs. To identify the genes influencing drug-specific sensitivity, we used a pooled collection of 6709 barcoded knockout *E. coli* strains covering 3500 nonessential genes. We determined the concentration needed to achieve 50% growth inhibition (IC_{50}) of wild-type *E. coli* for each drug. Drugs with low toxicity (IC_{50} > 50 μM) were used at a concentration of 50 μM. We removed eight drugs from the panel for technical reasons (table S1B). In three replicates, we inoculated the strain collection into minimal media with or without the drugs and terminated the screen when controls approached stationary phase (Fig. 1C). We sequenced the barcodes from extracted DNA and calculated the frequency of each knockout. We identified 191,552 statistically significant depleted or enriched knockouts relative to the no-drug control [FDR-adjusted

Department of Systems Biology, University of Massachusetts Medical School, Worcester, MA, USA.
*Corresponding author. Email: amir.mitchell@umassmed.edu

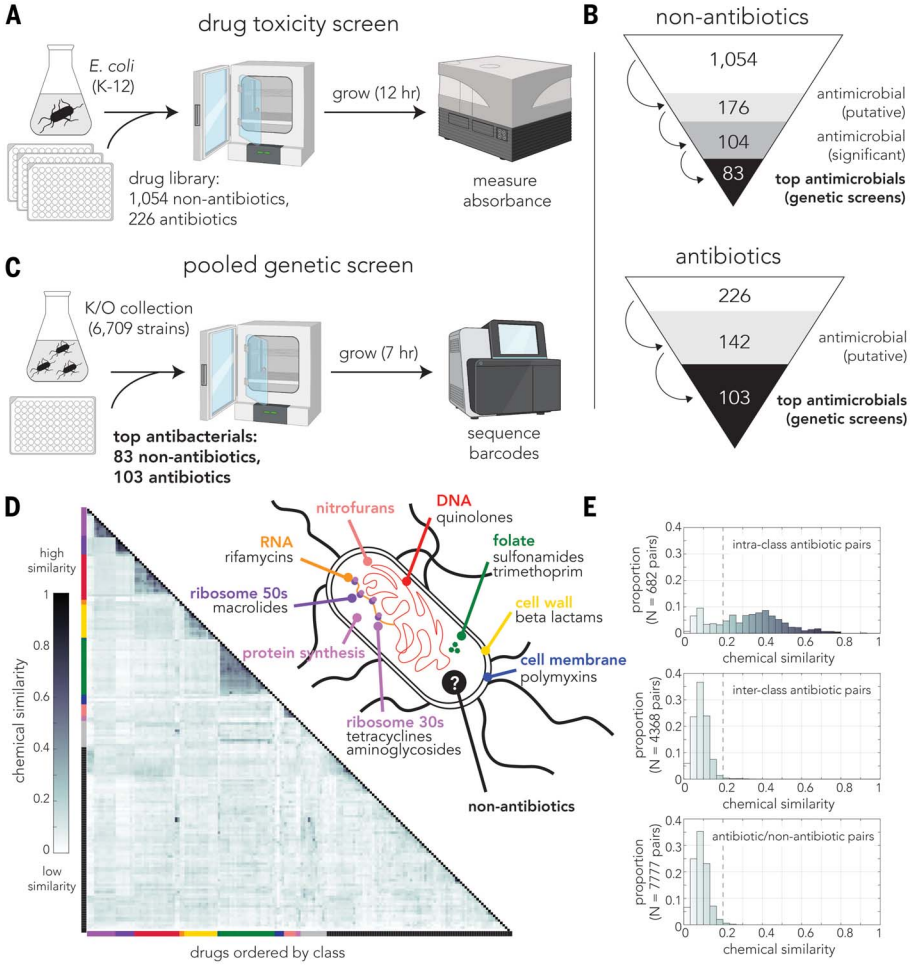

Fig. 1. Screening drugs for antibacterial activity. (**A**) Overview of drug screens. Overnight culture was diluted into minimal media aliquoted with a panel of 1280 drugs at a single concentration, and toxic drugs were identified by reduced growth. (**B**) Results from antibacterial activity screens with nonantibiotic and antibiotic drugs. Putative antimicrobials identified by the first screen were validated with a secondary screen, and top validated antimicrobials were used for the genetic screens. (**C**) Overview of pooled genetic screens. An overnight pooled collection of 6709 barcoded stains was diluted into minimal media aliquoted with 186 drugs and grown until control cultures reached late log phase. DNA was extracted, and barcodes were amplified by polymerase chain reaction (PCR) before sequencing. Screens were performed in triplicates. (**D**) Pairwise chemical similarity across all toxic drugs. The heatmap shows the Tanimoto coefficient with Morgan2 fingerprints of all drugs screened, sorted by drug class, and clustered within the class. (**E**) Histogram of pairwise chemical similarity across drug groups. Scores below 0.2 were considered chemically dissimilar.

P value < 0.25, Wald test in the DESeq2 program (*21*)]. Depleted knockouts reflect gene loss of function that increases drug sensitivity, whereas enriched knockouts reflect loss of function that increases resistance (all results are in table S3).

Known toxicity mechanisms are captured for standard antibiotics

We validated our method by verifying that it correctly identifies the known modes of action of 90 well-characterized antibiotics. Specifically, we chose a subset of knockouts (581 strains) that we expected would be informative for identifying shared modes of action by filtering out strains that rarely modulated toxicity (hits in less than two antibiotics) and strains that modulated toxicity very frequently (hits in more than 30 antibiotics). We also discarded knockouts of specific biological functions, such as efflux pumps, that can hinder the analysis of the mode of action (table S4). Figure 2A shows the results of hierarchical clustering of the informative strains. We observed that clustering was highly successful in recapturing antibiotic classes (shown by the colored dendrogram at the top of the heatmap): Seventy-five antibiotics were grouped into "pure" clusters with a single antibiotic class. All four cell-membrane targeting antibiotics were in a single mixed cluster.

Focusing on top hits of individual clusters uncovered many genes from the known target pathways (Fig. 2A, right side). For example, knockouts disrupting the SOS response and DNA repair (e.g., *recA* and *recN*) increased sensitivity to DNA-targeting antibiotics (red and pink clusters), whereas knockouts disrupting nucleotide excision repair, such as *uvrABC*, only increased sensitivity to nitrofurans (pink cluster) that induce DNA adducts requiring distinct repair mechanisms (*22*). For folic acid–targeting antibiotics, deletions in *folX* and *folM* increased resistance, whereas deletions in the glycine cleavage system (*gcv* genes) increased sensitivity (*23*). Knockouts disrupting peptidoglycan recycling increased sensitivity to cell-wall–targeting antibiotics.

To explore the relationship between antibiotic classes, we calculated the Pearson correlation between each pair of antibiotics (Fig. 2A, columns) and generated a graph representing drug relatedness. Figure 2B and fig. S1A show the drug similarity network (network layout was set with a force-directed algorithm by the strength of drug-drug correlations). Similarly to hierarchical clustering, this analysis grouped most antibiotics by their mechanism of action. However, the graph-based analysis also highlighted interclass relatedness that cannot be explained by chemical similarity (Fig. 2B, blue edges). Interclass relatedness inferred from the screens reveals shared pathways modulating the drug toxicity that extend beyond the antibiotic target. DNA-targeting antibiotics emerged as a network hub. Relatedness between classes was also supported by a separate approach—functional enrichment (Fig. 2B, margins, and table S5). This analysis revealed that cellular pathways known to be related to one class are also enriched in seemingly unrelated classes, such as DNA-related categories enriched in ribosome-targeting antibiotics.

Taken together, our results verified our approach for capturing the established mechanisms of action of standard antibiotics. The analysis revealed the value of this approach in uncovering higher-order interactions between antibiotic classes that have different cellular targets yet affect common pathways that modulate toxicity.

Antibacterial activity of nonantibiotics differs from that of standard antibiotics

We sought to identify the toxicity mechanisms of nonantibiotics by adding them to the drug-relatedness network that we generated for antibiotics. This analysis adds more nodes (drugs) and edges (relatedness interactions) to the network without altering the topology among antibiotics. In this analysis, nonantibiotics that target similar pathways to those of standard antibiotic classes would cluster with antibiotic network modules (Fig. 3A). However, we observed that most nonantibiotics remained completely unconnected to the antibiotic modules (57/77). The notable exceptions were 14 nonantibiotics that were connected to multiple

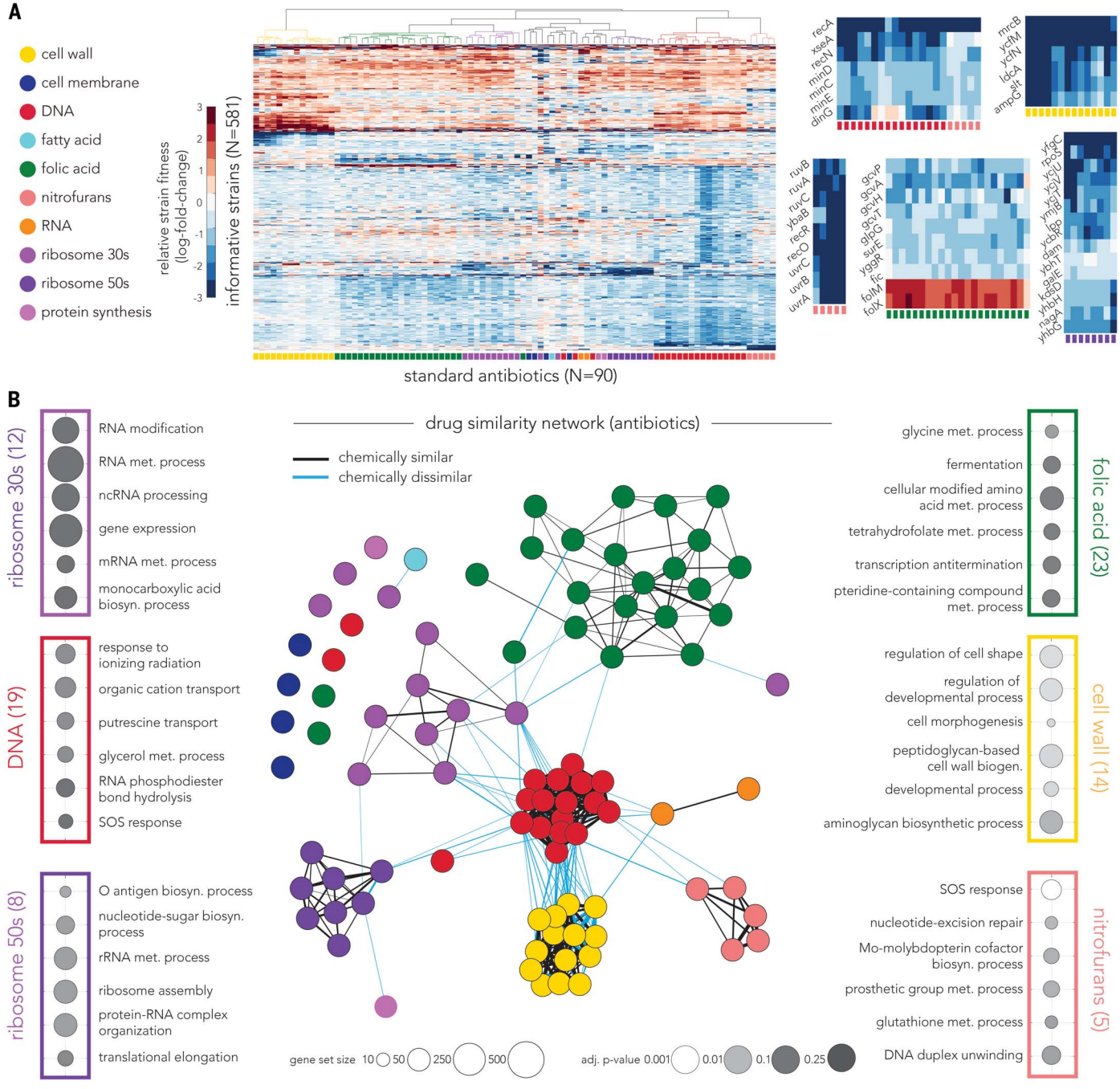

Fig. 2. Genetic screens capture antibiotic mechanisms of action and reveal interclass interactions. (**A**) Hierarchical clustering of antibiotics by the fitness score of informative knockouts. The colored squares at the bottom row indicate the class of each antibiotic and show that the algorithm successfully grouped most antibiotics into class-specific clusters. The right panels highlight signature knockouts characteristic to specific clusters. (**B**) Network representation of antibiotic drug resemblance by informative knockouts. Drug-drug correlations in knockout fitness were used as the measurement of resemblance, and the network was generated with a force-layout algorithm according to the correlation scores. Node and frame colors mark the antibiotic class. Most antibiotics self-grouped into the same class of network modules. The side panels show functional enrichment analysis by GO biological process terms of each module. Circle size and shading mark the size of gene set and statistical significance, respectively. ncRNA, noncoding RNA; met., metabolic; biosyn., biosynthetic.

antibiotic classes (positioned between the colored modules). When focusing on 52 chemically similar antibiotic and nonantibiotic pairs (Tanimoto coefficient >0.2), we did not detect high similarity in the genetic screen results (fig. S2A). To substantiate this conclusion, we used an alternative and widely used approach for classifying the mode of action of nonantibiotics. Specifically, we trained a random forest classifier that relied on all knockout strains to predict whether drugs can be classified as belonging to specific antibiotic classes (this analysis circumvented our choice of informative knockouts). In agreement with our network analysis, we observed that although our

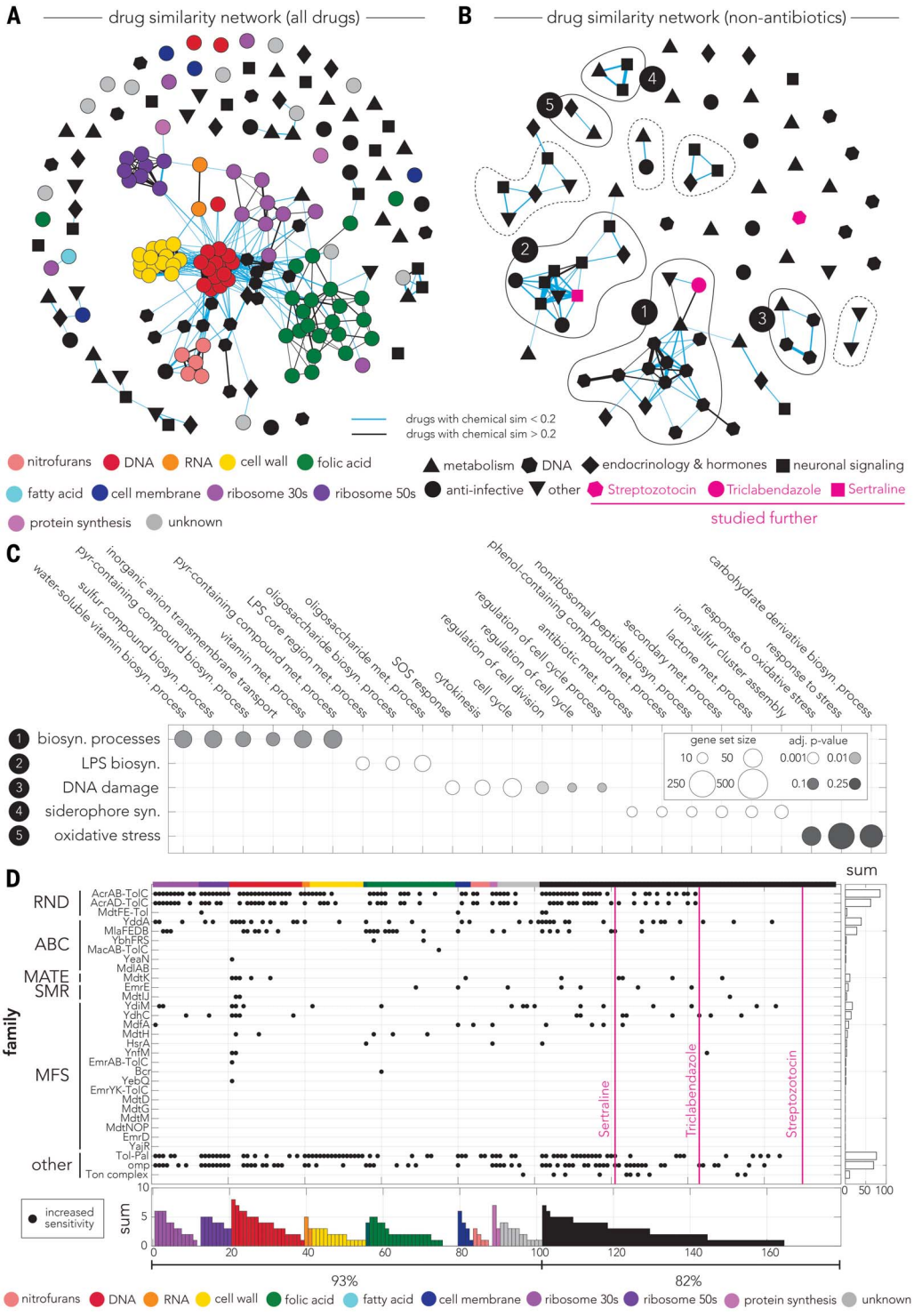

Fig. 3. Mechanisms underlying antibacterial activity of nonantibiotic drugs. (**A**) Network representation of resemblance across all drugs by 581 antibiotic informative knockouts. Node color marks the antibiotic class, and the node shape marks the drug use in host treatment. Only a few nonantibiotic drugs are clustered within antibiotic classes, indicating that most of them operate through different modes of action. (**B**) Network representation of nonantibiotic drug resemblance. The network was inferred by 509 nonantibiotic informative knockouts. Most drugs are associated with at least one neighbor, and many fall within clusters. Five clusters, marked by a continuous line, had statistically significant functional enrichment. Drugs marked in pink were further investigated. (**C**) Functional enrichment of nonantibiotic clusters by GO biological process terms. Circle size and shade mark the size of gene set and statistical significance, respectively. pyr, pyramidine; LPS, lipopolysaccharide. (**D**) The impact of knockouts in central drug-transport systems and membrane-permeability systems across individual drugs. Black circles represent statistically significant increased sensitivity. The colored bars at the bottom show the number of efflux and permeability systems that increased sensitivity for each individual drug. The white bars (right) show the number of drugs that have increased sensitivity for each individual efflux and permeability system. Drugs marked in pink were further investigated. The colors mark antibiotic class as shown in (A). ABC, adenosine triphosphate (ATP)–binding cassette; MATE, multidrug and toxic compound extrusion; SMR, small multidrug resistance; MFS, major facilitator superfamily.

classifier successfully assigned most antibiotics to their correct class, it failed to classify most nonantibiotics (fig. S2, B and C). Overall, the results indicate that nonantibiotic drugs likely operate through toxicity mechanisms that are orthogonal to standard classes of antibiotics.

The network analysis revealed that although most nonantibiotics were unconnected to antibiotic modules, some nonantibiotics are related to one another (Fig. 3A). This suggested that relatedness may exist but that it may be occluded by the antibiotic-centered analysis. We therefore repeated the network analysis, relying exclusively on knockouts that were informative for nonantibiotics (using similar filters as before). Figure 3B and fig. S1B show the resulting relatedness network that is based on drug-drug correlations across 509 informative knockouts. In this analysis, 52 of 77 nonantibiotics had at least one neighbor. Many connections were identified between drugs that are used for treating different human conditions and diseases (Fig. 3B, different node shapes), and most connections could not be explained by chemical similarity (Fig. 3B, blue edges).

We identified nine independent network modules and found that five modules were

enriched for specific biological functions (table S4). Figure 3C shows the top enriched Gene Ontology (GO) biological processes summarized by REVIGO (reduce and visualize Gene Ontology) (*24*, *25*). The largest module (14 drugs) was enriched for diverse biosynthetic and metabolic processes. This module included fluoropyrimidine chemotherapeutic drugs, which we previously characterized with similar findings (*15*). The second-largest module (10 drugs) was enriched in processes related to lipopolysaccharide biosynthesis. The third module was enriched in processes related to DNA damage repair and the stress response, and the two smallest modules included processes related to oxidative stress and siderophore-biosynthesis pathways.

Taken together, results from analyses of nonantibiotic drugs indicated that their antibacterial mechanisms are largely distinct from those of standard antibiotics. Moreover, our network analysis showed that nonantibiotics are not completely distinct from one another but that most of them can be grouped into modules reflecting shared toxicity mechanisms. This conclusion is further supported by the functional enrichment analysis, which uncovered common pathways modulating antibacterial activity. In addition, the modular network structure indicates that unexploited yet robust cellular targets for inhibiting bacterial growth may exist and provides multiple lead molecules for further investigation.

Transport systems affect both antibiotics and nonantibiotics

Our network analyses purposefully disregarded genes encoding efflux pumps, because they are expected to affect the antibacterial activity irrespective of the compound's target. We subsequently examined the impact on antibacterial activity of genes involved in membrane permeability and transport (76 genes from 33 pathways of drug transport and membrane permeability, table S4). Figure 3D shows interactions identified across all the drugs tested, as well as the pathways that increase bacterial sensitivity upon deletion. The widest impact on toxicity was observed for mutations affecting the resistance-nodulation-division (RND) family transporters, the Tol-Pal system, and outer membrane proteins (OMP). We observed that drugs varied considerably in the number of interactions that they have with transport systems, with 26 drugs affected by five or more different transport systems (specificity of pumps to antibiotic classes is shown in fig. S3). Overall, we observed that mutation in at least one transport system increased the antibacterial activity of 93% of antibiotics and 82% of nonantibiotics (Fig. 3D). This observation implies that evolved resistance against nonantibiotic drugs can potentially, in some cases, inadvertently lead to multidrug resistance and undermine the efficacy of antibiotics. Increased risk of unintentional cross-resistance may exist for nonantibiotic drugs that are affected by multiple transport systems.

Evolved resistance against nonantibiotic drugs

Our genetic screens, coupled with network analysis, have led to two important conclusions. First, the orthogonality in toxicity mechanisms indicates that nonantibiotics may potentially uncover unexploited targets for inhibiting bacterial growth. Second, analysis of drug-transport systems indicates that despite this orthogonality, broad resistance to antibiotics can emerge if drug transport–based resistance evolves as a result of selection by nonantibiotics. We tested these predictions experimentally by selecting for drug resistance in evolution experiments (*26*) (Fig. 4A). We focused on three nonantibiotics selected from different modules in the nonantibiotic network: streptozotocin, triclabendazole, and sertraline (Fig. 3B). Information about the toxicity of these drugs across representative microbiome species and five *E. coli* strains is provided in table S6.

Figure 4B shows the drug sensitivity curves of the ancestor strain and of five independently evolved clones. Streptozotocin- and triclabendazole-adapted clones were fully resistant to the drugs, whereas sertraline-adapted clones increased resistance by more than twofold. We sequenced the genomes of evolved strains to uncover the mechanisms underlying resistance. Figure 4C shows the mutations that we identified with the breseq tool (*27*). We used genes mutated across independent clones as evidence for likely driver mutations (Fig. 4C, dark-pink dots). Further support was provided by overlap of mutations with genetic-screening hits (Fig. 4C, light-pink dots).

We found three representative adaptation strategies for resistance. We identified numerous mutations in streptozotocin-evolved clones with a clear location bias toward the origin of replication. Streptozotocin, a naturally occurring alkylating agent that is used to treat pancreatic neuroendocrine tumors (*28*), repeatedly selected for inactivation of *nagE*, which encodes for glucose-6-phosphate transporter. This transporter is likely central for drug import and was previously observed to confer streptozotocin resistance (*29*). Clones adapted to triclabendazole, a drug used for treating worm infections, had only a handful of mutations. However, all independently evolved clones shared an in-frame mutation in a specific region of the essential gene *infB*, which encodes the translation initiation factor IF2. Previous work on lamotrigine, a drug that we identified as a triclabendazole neighbor in the drug-relatedness network (Fig. 3B), found that it binds to the same region of IF2 (*30*). Last, all sertraline-adapted clones had mutations in key regulators of efflux pumps (*marR*, *acrR*, and *lon*). Mutations targeting these regulators were very recently reported in sertraline-adapted strains and were shown to increase expression of multiple efflux systems (*31*). Our genetic screens also showed that sertraline, more than triclabendazole and streptozotocin, is sensitive to inactivation of transport systems (Fig. 3D).

Given the bacterial adaptation strategies that we observed, we predicted that sertraline-adapted clones, but not other clones, will emerge as multidrug resistors. Experiments measuring the resistance against a panel of antibiotics confirmed this prediction (Fig. 4D). In addition, given the hypothesis that triclabendazole binds to IF2, we predicted that triclabendazole-adapted clones will also be resistant to neighboring drugs in the relatedness network (fig. S4A). Drug-sensitivity measurements confirmed this prediction by showing that triclabendazole-evolved clones were also resistant to lamotrigine and pyrimethamine (fig. S4B). Furthermore, compound binding SEC-ASMS assays (size exclusion chromatography followed by affinity selection-mass spectrometry) confirmed that all three drugs bind the IF2 protein (fig. S4C).

The results from our evolution experiments uncovered instances of three representative strategies for adaptive resistance: decreased import, mutation of target, and increased export. However, beyond the specific mechanisms of action, the evolution experiment substantiated the two main premises arising from our work: (i) that orthogonality in modes of action can be leveraged to uncover proteins not currently used as targets by standard antibiotics and (ii) that despite orthogonality, adaptation against nonantibiotics can emerge through changes in drug efflux and therefore inadvertently culminate in antibiotic cross-resistance.

Discussion

Human health and microbiome integrity are tightly interlinked. This fundamental realization is the basis of current efforts to identify correlations between a myriad of environmental factors—such as diet and medication—and microbiome species composition. Although the widespread antibacterial activity of nonantibiotics is thought to be a key force underlying these associations, the modes of action of nonantibiotics in bacteria remain largely unknown. We addressed this gap in knowledge by developing a high-throughput genetic screening approach for systematically mapping interactions between dozens of antibacterial drugs and single-gene knockouts. Although a well-characterized lab strain of *E. coli* was an ideal platform for a high-throughput investigation of mode of action, additional work is needed to extend our study's conclusions to the human microbiome. Specifically, testing is necessary to determine whether nonantibiotics operate with similar modes of action in microbiome isolates and whether drug adaptation is observed in treated individuals.

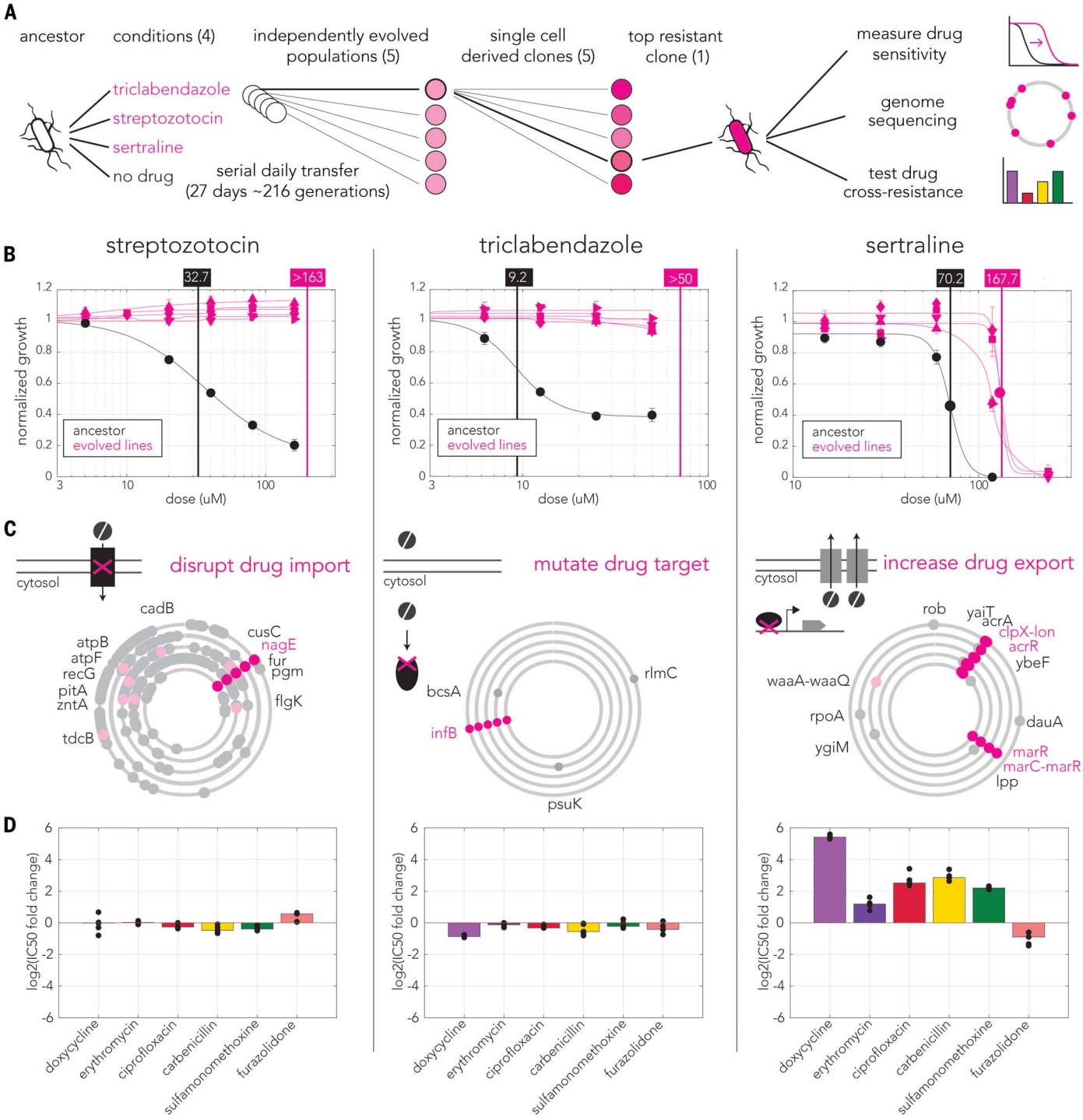

Fig. 4. Evolved resistance against nonantibiotics exposes unknown drug targets and collateral cross-resistance. (**A**) Overview of evolution experiment and downstream assays. Independent cultures were serially transferred in media supplemented with three nonantibiotics over 200 generations. A single resistant clone was isolated from each independently evolved population. (**B**) Drug resistance evolved across all cultures and drugs. The panels show the drug-sensitivity curves of ancestor and evolved clones; horizonal lines mark the concentration that inhibits growth by 50% (IC_{50}). (**C**) Results of whole-genome sequencing uncover three alternative strategies of evolved resistance. The concentric Circa plots represent the bacterial chromosome of individually evolved clones, and dots mark mutations. Dark-pink dots mark gene hits across at least four of the five replicates and likely adaptive mutations. Light-pink dots mark mutations in genes conferring drug resistance according to the genetic screen. The diagram on top represents the inferred mechanism of resistance. (**D**) Sertraline-evolved strains are resistant to multiple antibiotics, whereas triclabendazole- and streptozotocin-evolved strains do not confer cross-resistance. The panels show the increased resistance (IC_{50} fold-change) of evolved clones against six antibiotics. The bars represent the median across all evolved clones, and dots represent the mean of three biological replicates of each clone. The bar color shows the antibiotic class.

The network we constructed using drug-drug correlations recaptured the known antibiotic classes (Fig. 2B). When we added nonantibiotics to the antibiotic-centered clustering analysis, most of them remained unconnected, indicating that they do not inhibit *E. coli* through mechanisms similar to those of standard antibiotics (Fig. 3A). A subsequent analysis revealed that most of the nonantibiotics clustered into highly intraconnected modules enriched in specific cellular pathways (Fig. 3, B and C). Results from almost 200 drugs support the hypothesis that antibiotics and nonantibiotics target bacteria through orthogonal mechanisms of action. Network analysis focusing exclusively on nonantibiotics indicated that many of them share common toxicity mechanisms (Fig. 3B). Moreover, analysis of genes involved in drug transport indicated that despite orthogonality in mode of action, bacterial sensitivity to most drugs is increased by inactivation of transport systems and membrane-permeability proteins (Fig. 3D). The extensive impact of efflux systems on nonantibiotics is consistent with their known role in xenobiotic detoxification (*32*).

Our screen results showing orthogonality in toxicity suggest that nonantibiotics target bacterial cellular components not currently exploited by standard antibiotics. The modular network topology (Fig. 3B) further implies that some targets may be common to multiple nonantibiotics. This prediction is supported by our observations of triclabendazole-evolved resistance by in-frame mutations in IF2, a protein not targeted by standard antibiotics. Furthermore, confirming our network topology, we found that the two neighboring drugs in our network also bind IF2 (fig. S4). Another prediction, stemming from our finding of widespread sensitivity to inactivation of drug-transport systems, suggested that evolved resistance against nonantibiotics may confer broad drug resistance; this prediction was validated with sertraline-adapted strains (Fig. 4D). Although estimates of drug concentrations in the human digestive tract suggest that many nonantibiotics may apply a selective pressure on the gut microbiome, it remains to be determined whether adaptions will influence efflux pumps and inadvertently affect antibiotic resistance. Our results allow the gauging of nonantibiotics interacting with multiple efflux systems (Fig. 3D). This ranking can inform future studies focusing on specific interactions in the human microbiome.

The emergence and spread of antibiotic-resistant pathogens is a fundamental challenge for global health (*33*). Decreasing investment in development of new antibiotics in recent decades is only expected to compound the problem (*34*). Although technological advancements in robotic automation greatly increase the capacity to screen ever-growing libraries of small molecules (*35*), rediscovery of antibacterial compounds that belong to established antibiotic classes remains a bottleneck for innovation (*36*). This obstacle is common to both traditional natural product–based screening (*37*) and compounds proposed by artificial intelligence (*38*). Our methodology can be used to address this challenge because it can compare the pathways underlying antibacterial activity between hundreds of uncharacterized compounds and established antibiotics. As we showed, the results of these screens can be used for training classifiers to identify toxicity profiles that match established antibiotic classes. These classifiers can therefore also identify compounds operating through alternative, nonstandard modes of action.

REFERENCES AND NOTES

1. M. Zimmermann, M. Zimmermann-Kogadeeva, R. Wegmann, A. L. Goodman, *Nature* **570**, 462–467 (2019).
2. M. Zimmermann, K. R. Patil, A. Typas, L. Maier, *Mol. Syst. Biol.* **17**, e10116 (2021).
3. P. Spanogiannopoulos, E. N. Bess, R. N. Carmody, P. J. Turnbaugh, *Nat. Rev. Microbiol.* **14**, 273–287 (2016).
4. M. Klünemann *et al*., *Nature* **597**, 533–538 (2021).
5. G. Falony *et al*., *Science* **352**, 560–564 (2016).
6. A. Vich Vila *et al*., *Nat. Commun.* **11**, 362 (2020).
7. K. Forslund *et al*., *Nature* **528**, 262–266 (2015).
8. F. Imhann *et al*., *Gut* **65**, 740–748 (2016).
9. M. A. Jackson *et al*., *Nat. Commun.* **9**, 2655 (2018).
10. S. A. Flowers, S. J. Evans, K. M. Ward, M. G. McInnis, V. L. Ellingrod, *Pharmacotherapy* **37**, 261–267 (2017).
11. M. A. M. Rogers, D. M. Aronoff, *Clin. Microbiol. Infect.* **22**, 178.e1–178.e9 (2016).
12. L. Maier *et al*., *Nature* **555**, 623–628 (2018).
13. A. Tomasz, E. Borek, *Proc. Natl. Acad. Sci. U.S.A.* **46**, 324–327 (1960).
14. A. Tomasz, E. Borek, *Biochemistry* **1**, 543–552 (1962).
15. B. Rosener *et al*., *eLife* **9**, e59831 (2020).
16. A. P. García-González *et al*., *Cell* **169**, 431–441.e8 (2017).
17. H. L. Morgan, *J. Chem. Doc.* **5**, 107–113 (1965).
18. D. Rogers, M. Hahn, *J. Chem. Inf. Model.* **50**, 742–754 (2010).
19. M. Noto Guillen, B. Rosener, S. Sayin, A. Mitchell, *Cell Syst.* **12**, 1064–1078.e7 (2021).
20. S. Sayin *et al*., *eLife* **12**, e83140 (2023).
21. M. I. Love, W. Huber, S. Anders, *Genome Biol.* **15**, 550 (2014).
22. K. R. Ona, C. T. Courcelle, J. Courcelle, *J. Bacteriol.* **191**, 4959–4965 (2009).
23. R. J. Nichols *et al*., *Cell* **144**, 143–156 (2011).
24. M. Ashburner *et al*., *Nat. Genet.* **25**, 25–29 (2000).
25. F. Supek, M. Bošnjak, N. Škunca, T. Šmuc, *PLOS ONE* **6**, e21800 (2011).
26. J. E. Barrick, R. E. Lenski, *Nat. Rev. Genet.* **14**, 827–839 (2013).
27. J. E. Barrick *et al*., *BMC Genomics* **15**, 1039 (2014).
28. J. Capdevila *et al*., *Neuroendocrinology* **112**, 1155–1167 (2022).
29. J. Lengeler, *Mol. Gen. Genet.* **179**, 49–54 (1980).
30. J. M. Stokes, J. H. Davis, C. S. Mangat, J. R. Williamson, E. D. Brown, *eLife* **3**, e03574 (2014).
31. Y. Wang *et al*., *Proc. Natl. Acad. Sci. U.S.A.* **120**, e2208344120 (2023).
32. P. J. F. Henderson *et al*., *Chem. Rev.* **121**, 5417–5478 (2021).
33. C. J. L. Murray *et al*., *Lancet* **399**, 629–655 (2022).
34. M. A. Cook, G. D. Wright, *Sci. Transl. Med.* **14**, eabo7793 (2022).
35. L. Martínez-Fructuoso *et al*., *ACS Infect. Dis.* **9**, 1245–1256 (2023).
36. M. Miethke *et al*., *Nat. Rev. Chem.* **5**, 726–749 (2021).
37. T. M. Privalsky *et al*., *J. Am. Chem. Soc.* **143**, 21127–21142 (2021).
38. J. M. Stokes *et al*., *Cell* **180**, 688–702.e13 (2020).
39. M. N. Guillen, A. Mitchell, Mitchell-SysBiol./2024notoetal: v1.0.0, Zenodo (2024); https://zenodo.org/doi/10.5281/zenodo.10525157.

ACKNOWLEDGMENTS

We thank N. London and A. Orlov for their advice on measuring chemical similarity. We thank H. Youk and C. Navarro for their comments on the manuscript. **Funding:** This research was supported by National Institute of General Medical Sciences grant R35GM133775 (A.M.) and by National Institute of Allergy and Infectious Diseases grant R01AI170722 (A.M.). **Author contributions:** Conceptualization: A.M. and M.N.G. Methodology: A.M., M.N.G., B.R., and C.L. Investigation: M.N.G., B.R., and C.L. Visualization: A.M. and M.N.G. Formal analysis: A.M., M.N.G., and C.L. Funding acquisition: A.M. Project administration: A.M. Supervision: A.M. Writing – original draft: A.M. and M.N.G. Writing – editing: A.M. and M.N.G. Writing – review: A.M., M.N.G., B.R., and C.L. **Competing interests:** The authors declare that they have no competing interests. **Data and materials availability:** Raw sequencing reads from barcoded knockout library screen and whole genomes of evolved bacteria are available on the NCBI Sequence Read Archive under bioprojects PRJNA986181 and PRJNA998361. Cytoscape networks and the computer code (R and MATLAB) used in this article are deposited at Zenodo (*39*).

SUPPLEMENTARY MATERIALS

science.org/doi/10.1126/science.adk7368
Materials and Methods
Figs. S1 to S4
Tables S1 to S6
MDAR Reproducibility Checklist

Submitted 13 September 2023; accepted 4 March 2024
Published online 14 March 2024
10.1126/science.adk7368